Magnetic properties of transition metal fluorides MF_2 (M=Mn, Fe, Co, Ni) via high-energy photon diffraction

J. Strempfer,* U. Rütt, and S. P. Bayrakci
Max-Planck-Institut für Festkörperforschung, Heisenbergstrasse 1, 70569 Stuttgart, Germany

Th. Brückel
Institut für Festkörperphysik des Forschungszentrums Jülich, 52425 Jülich, Germany

W. Jauch
Hahn-Meitner-Institut, Glienicker Strasse 100, 14109 Berlin, Germany
(Received 31 July 2003; published 28 January 2004)

We present an overview of recent results from nonresonant magnetic diffraction experiments on the antiferromagnetic compounds MnF_2, FeF_2, CoF_2, and NiF_2 using high-energy synchrotron radiation of photon energies above 100 keV. New results are presented on the determination of the spin and of the L/S ratio for CoF_2 and NiF_2. For CoF_2, the saturation value of the long-range-ordered pure spin S_z component $S_z = 1.11(1)$ is considerably lower than the value $S_z = 3/2$ for the free Co^{2+} ion. This is in contrast to our results for NiF_2, where the full spin of the free transition-metal ion was found, $S_z = 0.98(1)$. The temperature dependence of the magnetization in the critical region as well as in the low-temperature region is also presented. For all compounds, Ising behavior is found in the critical regime, whereas the crossover to the low-temperature spin-wave behavior varies. We attribute this to different anisotropies in this series of compounds.

DOI: 10.1103/PhysRevB.69.014417 PACS number(s): 75.25.+z, 75.40.Cx, 78.70.Ck

I. INTRODUCTION

The transition-metal difluorides were investigated extensively in the fifties and sixties. Lately, renewed interest in MnF_2 has arisen, since it is an excellent material for study of the properties of the magnetic x-ray scattering cross section at high photon energies. It has been shown that the absolute magnetic moment can be deduced very reliably by this method.[1] Due to the high momentum space resolution, a very accurate determination of the critical exponent at the phase transition is possible.[2] Studies of the other transition-metal difluorides FeF_2,[3] CoF_2, and NiF_2 were subsequently undertaken. It became clear that interesting features related to the spin magnetic moment and the low-temperature behavior of the magnetic moment are present.

The fluorides we investigated all have the same tetragonal rutile-type crystal structure with space group $P4_2/mnm$ (see Fig. 2); NiF_2 develops a small orthorhombic distortion below T_N.[4] At low temperatures, MnF_2, FeF_2, and CoF_2 exhibit a two-sublattice antiferromagnetic ordering in which all spins are aligned along the tetragonal c axis. In NiF_2, the moments lie in the ab plane at an angle of about 0.9° to the b axis, resulting in a small ferromagnetic moment along the a axis.[5,6] Due to the non-symmorphic space group, the Bragg reflections of type $(h00)$ and (00ℓ) with h or ℓ odd are extinct in all compounds, allowing the measurement of the weak magnetic reflections at these positions.

In the series of transition-metal difluorides, only MnF_2 does not show an orbital contribution to the magnetic moment. This is as expected for a half-filled $3d$ shell. The other three compounds show a significant albeit quenched orbital contribution to the magnetic moment. This quenching is only partially lifted by the spin-orbit LS coupling.

Only with the development of the new synchrotron radiation sources it has become possible to use magnetic x-ray scattering as a method of separating spin (S) and orbital (L) moment contributions directly. The ratio L/S can be determined with nonresonant magnetic scattering in the regime of conventional hard x-ray energies (4–20 keV) by using polarization analysis. Here, one takes advantage of the different polarization factors of the spin and orbital components in the magnetic scattering cross section. This technique is accurate to about 10%.[7] By combination of these results with those from magnetic neutron diffraction, which measures the total magnetic moment (including spin and orbital part), the spin magnetic moment can be extracted. Other indirect methods of measuring the spin magnetic moment include nuclear-magnetic-resonance (NMR) and far-infrared absorption spectroscopy.[8,9]

In contrast, high-energy magnetic x-ray diffraction is sensitive only to the ordered spin component; the spin magnetic moment is measured directly. When the magnetic signal is normalized to the charge signal, this value can be determined on an absolute scale with an accuracy of about 2%.[3] This normalization technique is analogous to that of magnetic neutron diffraction, in which the absolute value of the total magnetic moment can be determined by normalizing the magnetic scattering to the nuclear signal.

The saturation values of the pure magnetic spin moments of MnF_2 and FeF_2 have already been determined by high energy x-ray diffraction.[1,3] It turns out that in these materials, the measured spin magnetic moment is, within error, identical to the spin moment expected for the free magnetic ion ($5\mu_B$ for MnF_2, and $4\mu_B$ for FeF_2). This is apparently not the case for CoF_2, for which both calculation and indirect measurements suggest an effective spin considerably lower than the free ion value of $S = 3/2$ for Co^{2+}. In this paper we

present an investigation of the spin magnetic moments of the remaining members of the series: CoF_2 and NiF_2.

In addition to determining the magnetic moment, we have investigated the magnetic phase transition, as well as the temperature dependence of the magnetic Bragg intensities. The investigation of the temperature dependence with high-energy x rays takes advantage of the high-momentum (Q) space resolution of x-ray diffraction at the synchrotron compared to that in neutron scattering experiments. Because of the narrow rocking curves of the Bragg reflections, the Bragg intensity can easily be separated from the much wider diffuse scattering background in the critical regime near the Néel temperature. Also, the separation of the weak magnetic reflections from Renninger reflections arising due to multiple scattering at the charge-forbidden positions is more easily done.

An introduction to high-energy x-ray diffraction is given in Sec. II. The formalism for obtaining the spin form factor is presented in Sec. III. In Sec. IV, the experimental setup and the properties of the CoF_2 and NiF_2 crystals are detailed. The results of the temperature-dependent measurements, as well as the determination of the absolute magnetic moment, are given in Sec. V. The corrections which have been applied are discussed. Finally, the results are discussed in Sec. VI and summarized in Sec. VII.

II. HIGH-ENERGY x-RAY DIFFRACTION

High-energy x-ray diffraction is complementary to neutron diffraction in many respects, mainly due to the low absorption of high-energy photons in matter. This allows us to investigate the bulk properties of the same materials with neutrons and high-energy x rays, even with the same sample environments.[10] Due to the high momentum space resolution of x-ray diffraction (on the order of 10^{-4} to 10^{-5} Å^{-1}), Bragg intensities can be separated very well from critical diffuse background. Critical phenomena can thus be investigated with great accuracy. We used high-energy magnetic x-ray diffraction as a probe to investigate the magnetic properties related to the pure spin moment and the magnetic phase transitions. The differential scattering cross section for magnetic diffraction for high photon energies above 80 keV takes the following simple form:[11]

$$\frac{d\sigma}{d\Omega} = r_0^2 \left(\frac{\lambda_C}{d} \right)^2 |S_\perp|^2, \tag{2.1}$$

where r_0 is the classical electron radius, λ_C the Compton wavelength, d the interplanar lattice spacing, and $S_\perp$ the Fourier transform of the spin component perpendicular to the diffraction plane. Because both the prefactors in Eq. (2.1) and the ratio of the number of unpaired electrons to the total number of electrons are small quantities, the magnetic signal for transition-metal compounds is typically six orders of magnitude smaller than the signal from charge scattering. For nonzero Q values, the next significant contributions arise from spin and orbital contributions in the scattering plane perpendicular to the scattering vector. These are insignificant in our scattering geometry because of the experimental configuration. In addition, these contributions are suppressed by $\sin\theta$ with respect to $S_\perp$ in the scattering cross section.[2] The validity of Eq. (2.1) for energies larger than 100 keV has been demonstrated experimentally[1] and later confirmed theoretically.[12] Hence, to a first approximation, no orbital contribution to the magnetic signal exists with this method. For neutrons, on the other hand, the diffracted intensity is proportional to the linear combination $\vec{L}(\vec{Q}) + 2\vec{S}(\vec{Q})$ of the Fourier transforms of the orbital and spin angular momenta. Thus, by combining the results of high-energy x-ray and neutron-diffraction experiments, orbital and spin contributions can be separated without further theoretical assumptions.

The high-energy scattering cross section (2.1) shows no polarization dependence. This implies that it is not possible to identify the magnetic character of a scattered signal by polarization analysis, as is possible for medium-energy x rays. It is, however, possible to identify the magnetic contribution from angular and temperature dependences.

Since the small magnetic intensities are diffracted purely kinematically, an enhancement due to the sample volume occurs. Maximum magnetic intensities are thus obtained for sample thicknesses on the order of the absorption length.

III. SPIN MAGNETIC MOMENTS FROM HIGH-ENERGY PHOTON DIFFRACTION

To obtain absolute values for the spin magnetic structure factor and thus the spin magnetic moment, it is necessary to normalize the measured magnetic intensities to a quantity which takes account of the reflectivity of the given crystal. Such a quantity is the charge-scattered signal, measured in exactly the same geometry as the magnetic signal. Nevertheless, to be able to use this signal for normalization, either the incident intensity has to be known very accurately or the charge structure factors have to be known. Since the first requirement is hard to fulfill at the synchrotron with the accuracy needed here, we used the second method.

Thus, in addition to the magnetic reflections, charge reflections have to be measured. The problem which arises here is the limited dynamical range of photon detectors. It is not possible to measure the weak magnetic signal and the strong charge signal in the same configuration. To measure the charge signal, the photon beam has to be attenuated, e.g., by thick iron absorbers, which have to be calibrated in order to obtain the true photon count rate (see Sec. V B). The absolute magnetic structure factor is then calculated from the magnetic and charge-scattered intensities according to the following equation which derives from Eq. (2.1), with incorporation of the geometry of the experiment and some sample properties:

$$|F_m|^2 = \frac{I_m}{I_c} \left(\frac{d}{\lambda_C} \right)^2 \frac{\sin 2\theta_m}{\sin 2\theta_c} |F_c|^2 \frac{y_{ext}}{W_m}. \tag{3.1}$$

Here I_m is the integrated magnetic intensity, I_c the integrated intensity of the charge reflections, and θ_m and θ_c are the Bragg angles of the magnetic and the charge reflections, respectively. F_c is the charge-density structure factor including the Debye-Waller factor, y_{ext} is the corresponding extinction

coefficient, and W_m is the Debye-Waller factor of the magnetic reflection. The most critical variable is y_{ext}, which must be determined experimentally (see Sec. V B).

The magnetic structure factor for a neutron diffraction experiment in the dipole approximation for transition metal ions is:[13]

$$F_m^n(Q) = g_z S f(Q) \tag{3.2}$$

$$= 2S[\langle j_0(Q)\rangle \tag{3.3}$$

$$+ (g_z/2-1)(\langle j_0(Q)\rangle + \langle j_2(Q)\rangle)], \tag{3.4}$$

with $g_z = \langle 0|L_z + 2S_z|0\rangle / \langle 0|S_z|0\rangle$ the gyromagnetic ratio, where $|0\rangle$ denotes the ground state wave function. In the case of high-energy x rays, only the first part (3.3) is measured, whereas the second part (3.4) represents the orbital contribution. High-energy magnetic diffraction and neutron diffraction are thus complementary probes which allow us to separate the spin and orbital components.

Finally, the magnetic structure factor $F_m(Q)$ is directly related to the magnetic moment by

$$\mu_{corr} = \frac{F_m(Q=0)}{N_m} \times \frac{S}{\langle S\rangle_0} \tag{3.5}$$

where N_m denotes the number of magnetic ions per unit cell and the fraction $S/\langle S\rangle_0$ denotes the correction for the zero-point reduction of the magnetic moment: the actual measured spin at zero temperature is $\langle S\rangle_0$ and the pure spin quantum number is S.

IV. EXPERIMENTAL DETAILS

The experiments on MnF_2 and FeF_2 were performed at the European Synchrotron Radiation Facility (ESRF) in Grenoble and the Advanced Photon Source (APS) at Argonne National Laboratory (ANL), respectively, and have been described elsewhere.[1,3] The experiments on CoF_2 and NiF_2 were conducted at the high-energy wiggler beamline of the Basic Energy Science Synchrotron Radiation Center[14] (BESSRC) and at the high-energy undulator station of the Midwest University Collaborative Access Team[15] (Mu-CAT) at the APS.

At BESSRC, an annealed Si(311) crystal ($\theta = 1.9°$, $\Delta\lambda/\lambda = 0.003$) was chosen as the monochromator. The crystal diffracts the wiggler beam horizontally into the experimental hutch, providing a photon energy of 115 keV and suppressing the second harmonic. The vertical scattering plane was defined by a second monochromator in the experimental station. To get maximum intensity, an annealed Si(220) monochromator with a rocking curve width of 6 arcsec at 115 keV was used. Since the rocking curve width of the CoF_2 (300) magnetic reflection is very narrow, with a full width at half maximum (FWHM) of 8.4 arcsec (see Fig. 1), the resolution function broadens the reflection width considerably. To determine the true rocking curve width of the sample, a perfect Si(220) crystal was used temporarily as second monochromator, with a rocking curve width of 0.4 arcsec at 115 keV. The rocking curve width of the magnetic

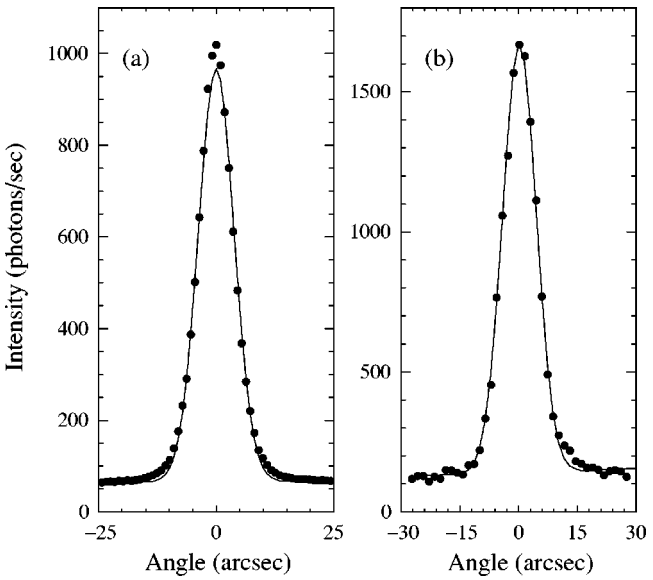

FIG. 1. Rocking curve of (a) the magnetic (300) reflection of CoF_2 at 5 K and (b) the magnetic (001) reflection of NiF_2 at 10 K. The FWHM's are 8.4 and 10.1 arcsec, respectively, using an imperfect Si(311) monochromator. The lines show a Gaussian fit to the data.

(300) reflection in this case was 6.8(5) arcsec FWHM. A liquid-nitrogen-cooled Ge solid-state detector was used, providing an energy resolution of about 300 eV. The beam size at the sample position was 1×1.5 mm^2.

The lattice constants of CoF_2 are $a = b = 4.6941$ Å and $c = 3.1698$ Å at 10 K.[16] The CoF_2 sample investigated is a single crystal with a thickness of 1.91(2) mm and a face of 2.3×2.2 mm^2. For the first experiment at BESSRC, it was mounted in an open-cycle helium-flow cryostat to reach temperatures as low as 4.6 K. The helium-flow cryostat has the advantage that it reaches slightly lower temperatures than a Displex and, even more importantly, that it has no vibrations. Vibrations would have made an absolute measurement of crystals of the quality of the CoF_2 crystal impossible, since they result in a rocking of the crystal by several arcseconds. While diffracting from (h00) reflections, the c axis of the crystal was oriented perpendicular to the diffraction plane. Since the magnetic moments in CoF_2 are aligned along the c axis (Fig. 2), the total magnetic spin moment was thereby

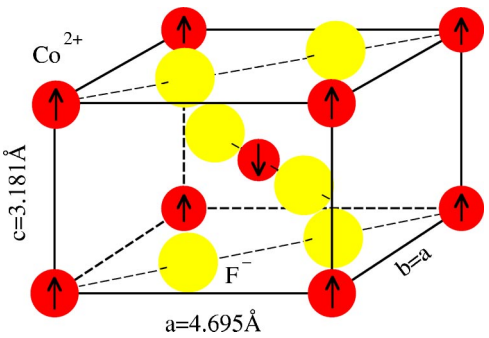

FIG. 2. Unit cell of CoF_2. The arrows show the directions of the magnetic moments in the antiferromagnetic phase.

measured [see Eq. (2.1)].

The experiment was conducted in bisecting mode. Thus, it was possible to use an additional axis, mounted on top of the ω circle and perpendicular to it, as a true Ψ rotation around the scattering vector. This was very convenient in order to avoid Renninger-reflections due to multiple scattering. Ψ scans, performed while maintaining the reflection condition, were used to find locations where no Renninger reflections were superposed on the magnetic reflections. Because of the small wavelength, the radius of the Ewald sphere is large, and thus the density of Renninger peaks along Ψ is high. Nevertheless, they can always be avoided by a Ψ rotation. This was discussed in detail in our study of MnF_2.[2]

The lattice parameters of NiF_2 at room temperature are $a=b=4.6478$ Å and $c=3.0745$ Å.[17] The magnetic moment below T_N lies in the ab plane with a small ferromagnetic moment along the a axis. Therefore, a different geometry had to be chosen. In addition, the crystal has to be rendered monodomain, since in the absence of an external magnetic field, the crystal forms [110]-twinned magnetic domains.[4] We used strong U-shaped permanent magnets to apply a 900 G field along the beam direction, thereby orienting the small a-axis ferromagnetic moments parallel to the beam. The crystal was mounted with the c axis in the scattering plane. The staggered antiferromagnetic moments were correspondingly oriented perpendicular to the diffraction plane, and therefore contributed maximally to the magnetically scattered signal in the (00ℓ) reflections.

A second experiment on CoF_2 was conducted at Mu-CAT. Here, a horizontally diffracting double monochromator was used. It was tuned to provide 50-keV photons in the first harmonic. The experiment itself was performed using the third harmonic of the monochromator, resulting in a photon energy of 150 keV. The experiment was conducted in the horizontal scattering plane. A cryocooled Ge solid-state detector was used. The CoF_2 crystal was mounted in an ''orange'' liquid-helium bath cryostat. In this case, the Ψ scans were performed with the ϕ tilt underneath χ, with ω in the bisecting geometry.

V. RESULTS

We present results on CoF_2 and NiF_2. These are the temperature dependence at low temperatures and in the critical region and the absolute spin magnetic moment. For comparison, they are shown together with previous results on MnF_2 and FeF_2.[2,1,3] In the case of the low-temperature behavior of the magnetic intensities and the magnetization we have reevaluated data from previous measurements on MnF_2 and FeF_2.

A. Temperature behavior

The temperature dependence of the (300) reflection of CoF_2 was investigated over the entire antiferromagnetic region, from 4.6 K up to the antiferromagnetic-to-paramagnetic phase-transition temperature $T_N=39.14(1)$ K. The smallest temperature step, just below T_N, was 0.1 K. The reduced magnetization $m=M(T)/M(0)$ was fitted by the power law $m=D\tau^{\beta}$, where $\tau=(1-T/T_N)$ is the reduced temperature and β the critical exponent. The fit to the data between 34 K and 0.1 K below T_N yields $\beta=0.306(6)$. The power-law fit is shown in Fig. 3 in double-logarithmic scale. The low-temperature behavior of the intensity of the CoF_2 magnetic reflections differs significantly from the behavior found for the other fluoride compounds but agrees well with the result plotted in Ref. 18 for the (100) magnetic reflection measured by neutron scattering, as seen in Fig. 4. The curve clearly cannot be described by mean-field theory, but instead shows a behavior closer to that of an Ising magnet.

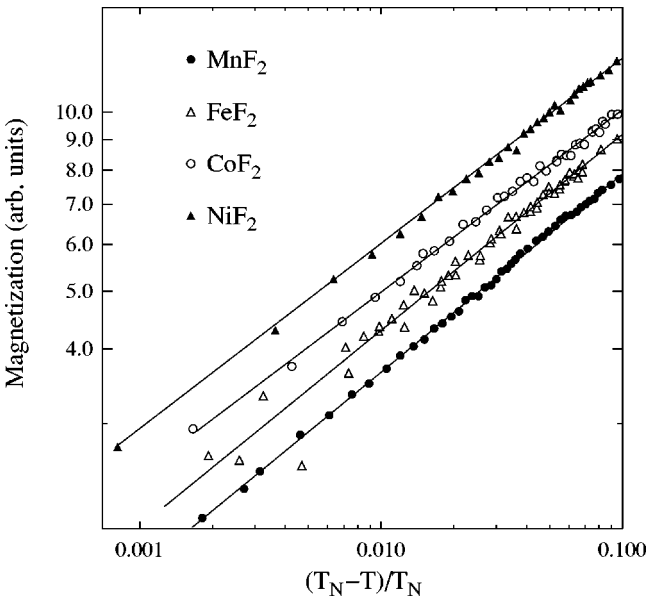

FIG. 3. Temperature dependence of the magnetization in the critical region in double logarithmic scale with the respective power-law fit.

The temperature dependence of the magnetization of NiF_2 in the critical region and over the full temperature range is shown in Figs. 3 and 5, respectively, together with those of MnF_2 and FeF_2. The intensities were determined from scattering of the (001) magnetic reflection between $T_N=12$ K and 74.12 K, with the magnetic field constantly applied in the a direction. From the fit to the data between 68 K and 0.1 K below T_N, we find $\beta=0.311(4)$ for the critical exponent, a value similar to that of CoF_2 (Fig. 3). The behavior over the full temperature range below T_N outside the critical region can be described quite well by the mean-field theory, as in the case for MnF_2 and FeF_2.

B. Absolute spin magnetic moment of CoF_2 and NiF_2

The magnetic (100) and (300) reflections of CoF_2 were measured at BESSRC at the lowest accessible temperature of 4.6 K. The integrated intensities were determined at several different positions in Ψ with $\Psi\sim 0$ (i.e., $S||(\hat{k}_i\times\hat{k}_f)$), and the c axis thus is perpendicular to the scattering plane. Here, $\hat{k}_i$ and $\hat{k}_f$ are the incident and scattered wave vectors, respectively. The integrated intensities were determined to an accuracy of 3% and 2%, respectively. In addition, (200) and (400) charge reflections were measured. These are used to normal-

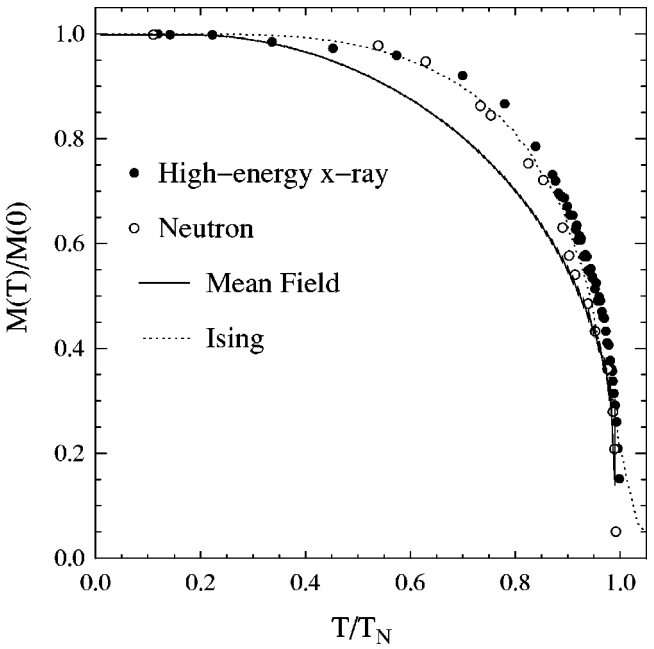

FIG. 4. Temperature dependence of the sublattice magnetization in CoF_2. The solid points show the data taken at the (300) reflection using 115-keV photons and the open circles are the values obtained by neutron scattering by Martel, Cowley and Stevenson (Ref. 18). The solid line represents the mean-field behavior for $S=3/2$ and the dashed line the Ising behavior.

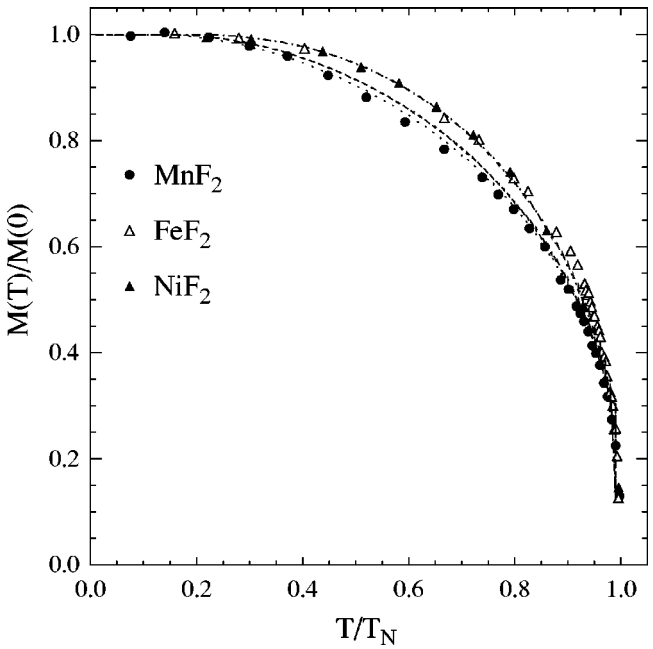

FIG. 5. Temperature dependence of the sublattice magnetization derived from the magnetic (300) reflection of MnF_2 and FeF_2 and from the (001) reflection of NiF_2, together with mean-field curves for $S=5/2$ (dotted line), $S=2$ (dashed line) and $S=1$ (dash-dotted line).

ize the magnetic reflections to obtain absolute magnetic moments according to Eq. (3.1). In order to eliminate possible systematic errors due to absorption, extinction, or dead time of the counting chain, the experiment was repeated under different conditions of photon energy and scattering geometry at the Mu-CAT beamline. Since the third harmonic was used in order to obtain 150 keV photon energy, it was not possible in this second experiment to measure the (300) reflection because the (100) reflection diffracts the main wavelength λ simultaneously. We instead used the (500) reflection, which could be measured very reliably.

For NiF_2, the magnetic (001) and (003) reflections were measured at $\Psi \sim 0$ with an accuracy of 3% and 8%, respectively. Here, the magnetic intensities were normalized to the charge intensities obtained from the (002) and (004) reflections.

The charge structure factors, which are essential for the determination of the absolute magnetic intensities, have been determined very accurately by γ-ray experiments at a photon energy of 316.5 keV using an ^{192}Ir source.[17] The values for the main $(h00)$ charge reflections for CoF_2, measured at 15 K and given in electron units are $F(200)=20.682$, $F(400)=29.954$, and $F(600)=21.218$.[19] The values for NiF_2 for the (00ℓ) reflections obtained for 15 K are $F(002)=53.159$ and $F(004)=25.793$.[17] These structure factors are corrected for extinction and include only the Debye-Waller factor.

The normalization requires different corrections to be applied to the charge intensities. At BESSRC, the dead time of the counting chain has been measured as 3.5 μs; this has been applied to the raw intensities. For the Mu-CAT experiment, a dead time of only 1.5 μs was determined, due to the smaller shaping time of the signal amplifier. The intensities of the charge reflections, which had to be measured with thick Fe attenuators, have been corrected to obtain the true intensities. The determination of the absorption coefficient at BESSRC was made by measuring the intensity with a variety of attenuator thicknesses, ranging from 51 and 69 mm. The absorption coefficient $\mu=0.2168(30)$ mm^{-1} was determined from the corresponding exponential fit. At Mu-CAT, a number of 3-mm-thick Fe-absorbers were calibrated individually. This results in an accuracy of the integrated intensities of the charge reflections of better than 2%.

Extinction turns out to be the most important correction involved in the determination of the absolute magnetic moment. However, while absorption can either be calculated very reliably or measured directly, extinction is not directly accessible by either method. The extinction correction for FeF_2 (rocking curve FWHM=45 arcsec) differs only by 1% when the Zachariasen[20] or the Becker and Coppens model[21] is used. The difference becomes more severe for the almost perfect CoF_2 or NiF_2 crystals, with intrinsic widths of $\eta=6.8(5)$ and $\eta=8.5(5)$ arcsec (FWHM), respectively. Here, the more accurate and refined model of Becker and Coppens must be used. The rocking curves of the magnetic reflections can be described quite well by Gaussians, as shown in Fig. 1 for the (300) reflection. The g value for a Gaussian mosaic distribution is $g=(2ln2/\pi)^{1/2}/\eta$. The extinction coefficients were determined for the (200) and (400) charge reflections of CoF_2 and the (002) and (004) reflections of NiF_2.

The extinction length $\Lambda=V_{uc}/(r_0\lambda|F_c|)$ is of the order of 80 μm, where V_{uc} is the unit cell volume. Since the mosaic

block size is much smaller (on the order of 1 μm), primary extinction effects associated with coherent scattering in an individual perfect crystal block are absent. Secondary extinction is the loss due to incoherent scattering from several different mosaic blocks. As shown in (Ref. 22), the type-I model (in which the mosaic block orientation dominates) can be applied. The extinction can then be determined directly from the parameter η. For CoF_2 the extinction is 42% and 44% at 115 keV and 29% and 31% at 150 keV for the (200) and (400) reflections, respectively. In the case of NiF_2, the extinction for the (002) reflection was severe because of the comparably very strong structure factor. The extinctions were 75% and 25% for the (002) and (004) reflections, respectively, but could nonetheless be accounted for by the Becker and Coppens extinction model very accurately with an estimated error of 4% in the extinction coefficient y_{ext}. The incident flux on the sample as determined from both reflections agrees to within 0.5%, which confirms the reliability of the correction.

In the determination of the absolute spin magnetic moments the smallest error is achieved by extrapolation if only the reflection with the lowest Q is used, e.g. (100). At this low-Q point, even a considerable difference of the form-factor behavior between the theory and the measured data at high Q has a very small effect on the extrapolation. Additional information can be obtained on the behavior of the form factor as a function of Q. Since only the spin component of the magnetic cross section is measured, $F_m(Q)$ should follow $\langle j_0 \rangle$ without the contribution of higher-order functions, as Eq. (3.3) shows. This allows us to evaluate possible contraction or expansion of the wave functions of the unpaired electrons with respect to the free-ion form factor, as has been reported in the case of NiO.[23,7]

The magnetic structure factor of CoF_2, calculated according to Eq. (3.1) with the above corrections applied to the charge intensities, is shown in Fig. 6. The 150-keV experiment at Mu-CAT confirmed the 115-keV BESSRC result, with reduced extinction. The magnetic structure factor determined from each experiment is given in Table I. The spin magnetic moment was obtained from a fit of the free ion form factor $f(Q)=\langle j_0(Q) \rangle$ to the structure factor values. Since $\langle j_0(Q=0) \rangle = 1$ by definition, the fit parameter gives the spin magnetic moment directly. The result is shown in Table I for each experiment separately (μ_S) and the two experiments combined ($\overline{\mu_S}$). In the determination of $\overline{\mu_S}$ the (100) value receives a considerably higher weighting. It should be noted that both experiments give exactly the same result. We take $\overline{\mu_S}=2.213(12)\mu_B$ as our final value, uncorrected for the zero-point motion. This corresponds to $S=1.107(9)$. The resulting value if a correction of the zero point motion of the moment of 2%, similar to FeF_2,[3] is applied, is $\mu_S^{corr}=2.258(15)\mu_B$. This value is 25% smaller than the value for the free Co^{2+} ion of $\mu_S=3\mu_B$.

The corresponding data for NiF_2 are also shown in Table I with the magnetic structure factor obtained from the fit shown in Fig. 7. The effect of the canting of the spins on the absolute value of the magnetic moment is negligible. The value of $\overline{\mu_S}=1.958(22)\mu_B$ is identical to the value of the magnetic moment of the free Ni^{2+}-ion of $\mu=2\mu_B$ if a 2% reduction due to zero-point motion is considered.

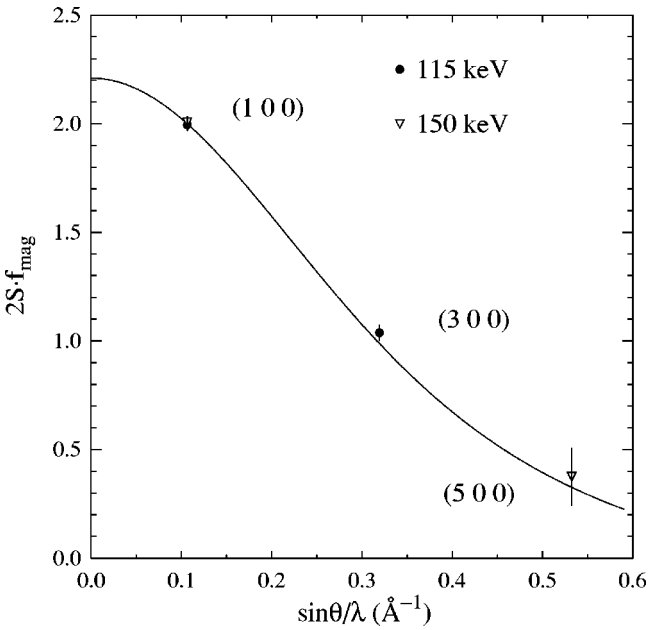

FIG. 6. Absolute magnetic structure factor of CoF_2 at $T=5$ K determined with 115-keV and 150-keV photons. The 115 keV data were taken on the (100) and (300) reflections. The 150-keV data were taken on the (100) and (500) reflections. The solid line shows a fit of $\langle j_0 \rangle$ for the free Co^{2+} ion to the data.

The estimated standard deviations given in Table I are due to statistical error in the count rates of the intensities and the uncertainties in the extinction and Debye-Waller factors. Systematic errors due to multiple scattering or the extinction model are not included in the numbers. They are estimated to lie in the range of 2–3% of the magnetic moments.

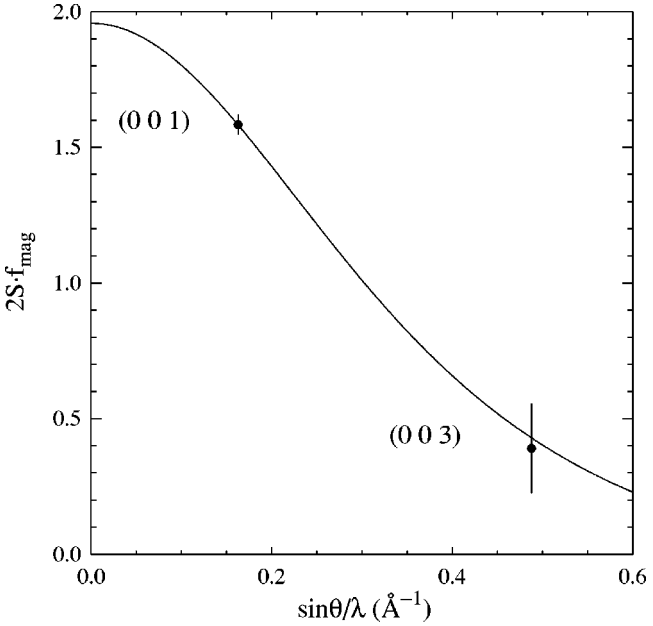

FIG. 7. Absolute magnetic structure factor of NiF_2 at $T=10$ K, determined with 115 keV photons. The solid line shows a fit of $\langle j_0 \rangle$ for the free Ni^{2+} ion to the data.

TABLE I. Magnetic structure factors $T=5$ K in electron units as derived from Eq. (3.1), using (a) the magnetic (100) and (300) reflections of CoF_2 from the BESSRC experiment and (b) the (100) and (500) reflections for the Mu-CAT experiment. Magnetic structure factors of NiF_2 are derived from the (001) and (003) reflections. The magnetic spin moment μ_S was obtained by fitting the respective $\langle j_0 \rangle$ function for each experiment to the data points separately, while the mean magnetic spin moment $\overline{\mu_S}$ is taken from a fit to all of the data from both experiments.

Compound	Reflection	F_m	μ_S (μ_B)	$\overline{\mu_S}$ (μ_B)
	(100)	1.994(13)		
CoF_2 (a)	(300)	1.037(35)	2.210(22)	
	(100)	2.007(27)		2.213(17)
CoF_2 (b)	(500)	0.38(13)	2.209(120)	
	(001)	1.584(35)		
NiF_2	(003)	0.389(163)	1.958(22)	

If the values of the experimentally determined magnetic structure factor are compared to the tabulated free ion form factor $\langle j_0 \rangle$, an expansion of the CoF_2 form factor by about 4% along the $a(b)$ axis can be deduced. In NiF_2, though the error bar of the (005) reflection is considerable, we consistently find a contraction of the magnetic form factor of about 4–7% along the c axis.

C. Comparison to spin magnetic moments of MnF_2 and FeF_2

In Table II, the measured spin magnetic moments for all four fluoride compounds are compared. For MnF_2, the magnetic structure factors given in Ref. 1 have been reevaluated using Becker and Coppens extinction model with Gaussian line shape. This gives a spin magnetic moment of $\overline{\mu_S} = 5.04(6)\mu_B$. This model is better adapted to the small rocking curve widths of this crystal then the Zachariasen model used previously. If a 2.5% reduction of the moment due to zero-point motion is considered,[24] this value becomes $5.16(6)\mu_B$. This is consistent with the free-ion value of $\mu = 5\mu_B$, if the systematic errors given in Ref. 1 are taken into account. The systematic error due to a small contribution of multiple charge scattering for the magnetic Bragg intensities can, in the case of MnF_2, be comparable to the ESD from counting statistics, while it is estimated to be much smaller than $0.06\mu_B$ for the other compounds. Here, the magnetic moment was determined from the (300) reflection, since this reflection was measured most carefully. The value of $\overline{\mu_S} = 3.93(4)\mu_B$ given for FeF_2 is taken from Ref. 3. After correction for the zero-point reduction of the magnetic moment, we obtain $4.01(5)\mu_B$, which shows that the spin of the free Fe^{2+}-ion is preserved. All values given in Table II are presented without correction for the moment reduction due to the zero-point motion.

VI. DISCUSSION

In this paper we have combined results from CoF_2 and NiF_2 with previous data on MnF_2 (Refs. 2,1) and FeF_2 (Ref. 3). The latter have been reevaluated to take into account factors such as the low-temperature behavior of the magnetic intensity and in the case of MnF_2, the use of the Becker and Coppens extinction model, which is more adapted for the small rocking curve widths of this crystal.

As shown in Table II we find that all four compounds show Ising-type behavior in the critical region. For MnF_2 and FeF_2, this was discussed in Refs. 2 and 3 respectively. The value found for CoF_2 of $\beta = 0.306(6)$ agrees very well with the result $\beta = 0.305(30)$ obtained by Cowley and Carneiro,[25] who fit the power law only in a region of a few mK close to T_N. In the study presented here, this exponent was found to be valid over a region between $0.7T_N$ and T_N.

Our data on the spin magnetic moment of MnF_2, FeF_2, and NiF_2 confirm the ionic character of these compounds; the full free-ion moment is found. We cannot reproduce the results obtained by Brown, Figgis, and Reynolds[26,27] who suggest a spin depolarization due to a covalent bond fraction of 10% between Fe and F and 28% between Ni and F from polarized neutron diffraction and *ab initio* calculations of spin densities in the local density approximation. Our results agree with those of Palmer and Jauch,[17] who performed multipole refinement of γ-ray diffraction data at room temperature, as well as at 15 K and concluded that both compounds show ionic character.

In contrast, the spin magnetic moment measured for CoF_2 is considerably reduced from the free-ion value. For the four compounds, the electronic charge-density distributions have been studied using highly accurate structure factors measured with 316.5-keV γ radiation. In all cases, the total number of 3d electrons on the metal ion (i.e., the monopole population) turned out to be virtually identical with the formal integer values, e.g., $P(3d) = 6.95(3)e$ for CoF_2.[19] The spin reduction on Co therefore cannot be related to charge trans-

TABLE II. Spin quantum number S of the M^{2+} ion, together with the g_z value determined by other methods. This is compared to the mean value of the spin magnetic moment measured with high-energy x rays. The critical temperature T_N and exponent β as determined with high-energy x-ray diffraction are also listed.

	S	g_z	$\overline{\mu_S}$ (μ_B)	T_N (K)	β
MnF_2	2.5	2.00	5.04(6) (Ref. 1)	67.71(1)	0.333(3) (Ref. 2)
FeF_2	2	2.25 (Ref. 32)	3.93(4) (Ref. 3)	75.81(11)	0.329(18) (Ref. 3)
CoF_2	1.5	2.60 (Ref. 30)	2.21(2)	39.14(1)	0.306(6)
NiF_2	1	2.35 (Ref. 33)	1.96(2)	74.1(1)	0.311(5)

fer towards the ligands. It should be pointed out that considerable reductions were observed in the case of the transition-metal monoxides with valence monopole populations of 6.42(4) and 4.75(2) on the metal ion in CoO (Ref. 28) and MnO (Ref. 29). Instead of charge transfer, a mixture of high-spin and low-spin configurations in the $3d$ orbitals may occur in CoF_2, which could lead to a considerable reduction of the magnetic moment. Molecular-field calculations by Lines[31] give a effective spin of $S=1.09$, which is reduced to a value of $S=1.06$ by spin waves. Our findings strongly support this result. In this theory, only spin operators which describe the two lowest molecular field states have been included, but this seems already to describe our data very well.

When the temperature dependence of the sublattice magnetization in CoF_2 is compared to the temperature dependences of the other three compounds, it becomes clear that anisotropy, i.e., a nonquenched orbital contribution, is significant for CoF_2 and leads to more rapid saturation. Unlike MnF_2, in which the anisotropy field acting on the Mn^{2+} ion is much weaker than the exchange field, for CoF_2 the opposite is true. Therefore, a totally different magnetic behavior and a reduction of the spin magnetic moment is quite possible. The CoF_2 g factor of $g=2.60$ calculated by Khan *et al.*[30] clearly shows a considerable contribution of an orbital moment to the total magnetization. It is larger than the values corresponding to the other three compounds, as shown in Table II.

A neutron magnetic-moment determination performed by Erickson resulted in a g factor of $g=2$ ($3\ \mu$B) for CoF_2.[34] If we consider the real orbital contribution described by the actual g factor of $g=2.6$ mentioned before, we arrive at a value for the pure spin of 1.15 which is virtually identical with our value of $S_z=1.129(9)$. This result is supported by indirect measurements of the time-averaged spin $\langle S_z\rangle_0$ by NMR (Ref. 8) and far-infrared absorption spectroscopy.[9] These methods determine the spin, via the ground-state splitting; they produce the results $\langle S_z\rangle_0=1.3$ and 1.13.

The expansion and contraction of the magnetic form factor along the Q axis found for CoF_2 and NiF_2 have not yet been confirmed by other methods.

Finally, we want to comment on the applicability of this method to other compounds. Its limits arise from the fact that the nonresonant magnetic x-ray scattering cross section is rather small compared to charge scattering and background signal. The observation of nonresonant Bragg scattering is in principle possible for a range of samples. However, in our view the most important information that can be obtained is the determination of the pure spin form factor. Its precision measurement described here relies on (i) the high crystal quality, (ii) the rather large magnetic moments, (iii) the favorable ratio of the number of unpaired electrons, to the total number of electrons and (iv) the simple domain state of the compounds under investigation. In this respect, the transition metal difluorides are extremely well suited.

VII. SUMMARY AND CONCLUSIONS

We have reported measurements of the absolute spin magnetic moment and the temperature dependence of the nonresonant magnetic intensities in CoF_2 and NiF_2, and compared these to earlier results on MnF_2 and FeF_2.

MnF_2, FeF_2, and NiF_2 behave quite classically. The spin magnetic moment at saturation corresponds to the free-ion value, if a reduction due to zero-point spin fluctuations is taken into account and the overall temperature dependence follows a mean-field behavior. This demonstrates the dominant ionic character of these compounds. CoF_2, on the other hand, shows a significant reduction of the spin magnetic moment in saturation: 25% compared to the value of the free Co^{2+} ion. The overall temperature dependence differs significantly from a mean-field curve and indicates a strong crystal-field anisotropy. We attribute this behavior to a nonquenched orbital contribution which also causes the g values which differ significantly from 2. In the critical region, on the other hand, all four compounds show critical exponents β characteristic of an Ising-type universality class. Finally, we find a contraction and expansion of the spin-density distribution compared to that of the free ion for the compounds CoF_2 and NiF_2. This is a typical solid-state effect.

We conclude that nonresonant scattering of high-energy x rays provides highly precise and detailed information on the spin density which can serve as test data for density-functional theories of these rather simple compounds.

ACKNOWLEDGMENTS

This work has been supported by the Department of Energy, Office of Basic Energy Sciences, Division of Materials Sciences, under Contract No. W-31-109-ENG-38 and the State of Illinois under HECA. Use of the Advanced Photon Source was supported by the U.S. Department of Energy, Office of Science, Office of Basic Energy Sciences, under Contract No. W-31-109-Eng-38. The Midwest Universities Collaborative Access Team (MUCAT) sector at the APS was supported by the U.S. Department of Energy, Office of Science, Office of Basic Energy Sciences through the Ames Laboratory under Contract No. W-7405-Eng-82.

*Email address: J.Strempfer@fkf.mpg.de.

[1] J. Strempfer, Th. Brückel, D. Hupfeld, J.R. Schneider, K.-D. Liss, and Th. Tschentscher, Europhys. Lett. **40**, 569 (1997).
[2] J. Strempfer, Th. Brückel, U. Rütt, J.R. Schneider, K.-D. Liss, and Th. Tschentscher, Acta Crystallogr., Sect. A: Found. Crystallogr. **52**, 438 (1996).
[3] J. Strempfer, U. Rütt, and W. Jauch, Phys. Rev. Lett. **86**, 3152 (2001).
[4] A. Palmer and W. Jauch, Solid State Commun. **77**, 95 (1991).
[5] R.G. Shulman, Phys. Rev. **121**, 125 (1961).
[6] P.J. Brown and J.B. Forsyth, J. Phys. C **14**, 5171 (1981).
[7] V. Fernandez, C. Vettier, F. de Bergevin, C. Giles, and W. Neubeck, Phys. Rev. B **57**, 7870 (1998).
[8] V. Jaccarino, Phys. Rev. Lett. **2**, 163 (1959).
[9] S.J. Allen and H.J. Guggenheim, Phys. Rev. B **4**, 937 (1971).
[10] J.R. Schneider, R. Bouchard, Th. Brückel, M. Lippert, H.-B. Neumann, H.-F. Poulsen, U. Rütt, Th. Schmidt, and M.v. Zimmermann, J. Phys. IV **4** (C9), 415 (1994).

[11] M. Lippert, T. Brückel, T. Köhler, and J.R. Schneider, Europhys. Lett. **27**, 537 (1994).
[12] M. Colarieti-Tosti and F. Sacchetti, Phys. Rev. B **58**, 5173 (1998).
[13] P.J. Brown, ''Magnetic Scattering of Neutrons,'' in Int. Tables Crystallogr. C, edited by A.J.C. Wilson (Kluwer, 1992), p. 512.
[14] U. Rütt, M.A. Beno, J. Strempfer, G. Jennings, C. Kurtz, and P.A. Montano, Nucl. Instrum. Methods Phys. Res. A **467-468**, 1026 (2001).
[15] T. Brückel (unpublished).
[16] K. Haefner, Ph.D. thesis, University of Chicago, 1966.
[17] A. Palmer and W. Jauch, Phys. Rev. B **48**, 10 304 (1993).
[18] P. Martel, R.A. Cowley, and R.W.H. Stevenson, Can. J. Phys. **46**, 1355 (1968).
[19] W. Jauch, M. Reehuis, and A.J. Schultz, Acta Crystallogr., Sect. A: Found. Crystallogr. **60**, 51 (2004).
[20] W.H. Zachariasen, Acta Crystallogr. **23**, 558 (1967).
[21] P.J. Becker and P. Coppens, Acta Crystallogr., Sect. A: Cryst. Phys., Diffr., Theor. Gen. Crystallogr. **30**, 129 (1974).
[22] A. Palmer and W. Jauch, Acta Crystallogr., Sect. A: Found. Crystallogr. **51**, 662 (1995).
[23] H.A. Alperin, J. Phys. Soc. Jpn. **17**, 12 (1962).
[24] H. Yasuoka, T. Ngwe, V. Jaccarino, and H.J. Guggenheim, Phys. Rev. **177**, 667 (1969).
[25] R.A. Cowley and K. Carneiro, J. Phys. C **13**, 3281 (1980).
[26] P.J. Brown, B.N. Figgis, and P.A. Reynolds, J. Phys.: Condens. Matter **2**, 5297 (1990).
[27] P.J. Brown, B.N. Figgis, and P.A. Reynolds, J. Phys.: Condens. Matter **2**, 5309 (1990).
[28] W. Jauch and M. Reehuis, Phys. Rev. B **65**, 125111 (2002).
[29] W. Jauch and M. Reehuis, Phys. Rev. B **67**, 184420 (2003).
[30] D.C. Khan, S.M. Kirtane, and J.K. Sharma, Phys. Rev. B **23**, 2697 (1981).
[31] M.E. Lines, Phys. Rev. **137**, A982 (1965).
[32] R.C. Ohlmann and M. Tinkham, Phys. Rev. **123**, 425 (1961).
[33] P.L. Richards, Phys. Rev. **138**, A1769 (1965).
[34] R.A. Erickson, Phys. Rev. **90**, 779 (1953).